DOI 10.24425/aee.2024.148854

Dead time effects compensation strategy by third harmonic injection for a five-phase inverter

KRZYSZTOF ŁUKSZA ✉, DMYTRO KONDRATENKO, ARKADIUSZ LEWICKI

Faculty of Electrical and Control Engineering, Gdańsk University of Technology
11/12 Narutowicza str., 80-233 Gdańsk, Poland
e-mail: {✉ krzysztof.luksza/dmytro.kondratenko/arkadiusz.lewicki}@pg.edu.pl

(Received: 25.07.2023, revised: 01.02.2024)

Abstract: This paper proposes a method for compensation of dead-time effects for a five-phase inverter. In the proposed method an additional control subsystem was added to the field-oriented control (FOC) scheme in the coordinate system mapped to the third harmonic. The additional control loop operates in the fixed, orthogonal reference frame ($\alpha - \beta$ coordinates) without the need for additional Park transformations. The purpose of this method is to minimize the dead-time effects by third harmonic injection in two modes of operation of the FOC control system: with sinusoidal supply and with trapezoidal supply. The effectiveness of the proposed control method was verified experimentally on a laboratory setup with a prototype five-phase interior permanent magnet synchronous machine (IPMSM). All experimental results were presented and discussed in the following paper.

Key words: dead-time effects, field-oriented control, five-phase voltage source inverter, IPMSM, sensorless control

1. Introduction

For the last few decades there has been an ever-growing interest in drive systems with multi-phase electric machines. The term "multi-phase machine" refers to any type of electric machine with a number of phases higher than three, e.g. five-phase, seven-phase, eleven-phase etc. Although the concept of such machines is not a new one, as it dates back to the late 1960s [1], it has not yet found a wide range of practical applications, possibly due to the fact, that such motors generally have to be supplied from multi-phase inverters, specifically designed for powering such machines. However, multi-phase machines can utilize certain phenomena not present in classical three-phase machines, which can offer certain benefits in comparison with classical ones, such

as [1–5]: higher fault tolerance (a multi-phase motor can continue to operate with one or more phases open circuited, although with a substantially derated power), reduction of the rated phase currents of power converter devices for the same generated power (less powerful transistors can be used), smaller torque ripple, smaller operating noise and higher torque density thanks to the injection of the higher harmonics of supply voltage (only in the case of machines with an odd number of phases).These properties are especially beneficial for applications where high reliability is especially important, such as: electric and hybrid vehicles, electric ship propulsion, locomotive traction vehicles etc. Multi-phase machines can be constructed as both induction and synchronous. Induction machines are the most commonly used thanks to their simpler control methods. However, for safety critical applications (e.g. "more-electric" aircraft) permanent magnet synchronous machines with modular windings are used [1, 2, 6].

Inverter fed drive systems with AC electric machines require the usage of pulse width Modulation (PWM) strategies. These methods assume the usage of ideal power electronics switches, whose commutation times and voltage drops are equal to zero [7]. In real systems, despite constant development in the field of power electronics such requirements are not yet possible to meet. Thus, due to non-zero turn-on and turn-off times of power transistors, an amount of dead-time dependent on the transistor switching period has to be set in order to prevent short-circuiting the dc link voltage sources by simultaneously switching on upper and lower transistors. The dead-time delays the activation of the next transistor until the previous one in the same inverter branch is fully deactivated [7]. Although such safety precautions are essential, the dead-time causes voltage distortion, such as e.g. increase in the harmonic content of the inverter output, decreasing the quality of the supply voltage [8].

Several solutions to solve the problem of dead-time effects have been proposed. In general, two approaches were utilized: PWM with low order harmonic reduction [9–14], or additional controllers in the control scheme [15–18]. However, these solutions were tested for single and three-phase drive systems, while the multi-phase case was considered in [19], where the specific phenomena appearing in a multi-phase machine supplied by a VSI were described. The dead-time effect causes the appearance of 5^{th} and 7^{th} harmonics in three-phase systems, while in five-phase systems the 3^{rd} and 7^{th} harmonics appear. The harmonics of higher order are limited by the load inductance.

In multi-phase systems, when utilizing the same dead-time compensation methods as for three-phase systems, the low-order harmonics content is significantly higher. In a five-phase drive system, when operating without third harmonic injection, just as in the case of three-phase systems, the PWM must generate sinusoidal harmonic-free output voltages in order to avoid the appearance of low-order stator current harmonics [19]. Although PWM methods suitable for multi-phase VSIs have been developed [20, 21], which theoretically produce sinusoidal output voltages with no low order harmonics, in practice they do appear in the output voltages, and consequently currents, of the multi-phase VSIs [19].

The five-phase drive system investigated in the following manuscript uses a field-oriented control (FOC) scheme operating in two sets of coordinates, allowing for simultaneous control of both first and third harmonic currents. In the dead-time effect compensation method proposed in this paper an additional control subsystem was added to the FOC control scheme in the coordinate system mapped to the third harmonic. The additional control loop operates in the fixed, orthogonal reference frame ($\alpha - \beta$ coordinates). The subsystem uses the $\alpha - \beta$ components of the measured

currents for the third harmonic, already available in the control system, as feedback in the control loop, in order to generate $\alpha - \beta$ reference voltage components. When operating with sinusoidal voltage supply, the proposed approach is aimed to minimize the third and higher current harmonics. Thus, the waveforms of the resultant phase currents are significantly closer to purely sinusoidal. In the case of trapezoidal voltage supply, the system uses the difference between the $\alpha - \beta$ current components measured in the system and estimated by a state observer in order to generate $\alpha - \beta$ reference voltage components minimizing the disturbances, i.e. all the unwanted harmonic content, creating quasi-trapezoidal phase current waveforms. The main difference between the proposed and already existing dead-time effect compensation techniques is operating in the fixed $\alpha - \beta$ coordinate system, thus avoiding the need for two additional Park transformations.

The following paper is organized as follows: Section 2 describes the sensorless control scheme and the details of the proposed dead-time effect compensation method, Section 3 describes the laboratory experimental setup, Section 4 presents the results of the experimental studies, while Section 5 provides the conclusions as to the performance of the proposed dead-time effect compensation method.

2. Proposed control scheme

The proposed control system for sensorless control of a five-phase IPMSM consists of a dual-plane FOC control scheme with angle synchronization and a dead-time effect compensation subsystem. A block diagram of the complete structure of the proposed control system is presented in Fig. 1.

2.1. Dual-plane FOC control system for a 5-phase IPMSM

The dual-plane control scheme for sensorless control of the five-phase IPMSM proposed in this paper is based on a concept of a dual-plane control structure proposed in [22, 23] for controlling a five-phase squirrel-cage induction machine using multiscalar variables. The system includes a cascade structure of PI controllers of rotor speed and $d - q$ current components in two coordinate systems (planes): I (mapped to the first harmonic variables) and II (related to the third harmonic variables). The mechanical interpretation of this control scheme is a system of two three-phase machines connected by a common shaft, with the first one modelling the first (basic) harmonic variables (plane I), and the second, modelling the third-harmonic (plane II), which has a three times higher number of poles and revolves in the opposite direction.

For the purpose of the third harmonic injection the control scheme contains an angle synchronization subsystem. The system executes angle transformation between the two planes, while an angle controller synchronizes the position of the rotor flux vectors of both systems in order to achieve a quasi-trapezoidal resultant rotor flux.

The proposed FOC control system operates without speed and position sensors, using two separate speed observers to estimate rotor speed and position for planes I and II. Observers implemented here have the structure of an adaptive full-order observer, presented in [24, 25]. Nevertheless, each observer operates on a different set of parameters, for the I and II planes.

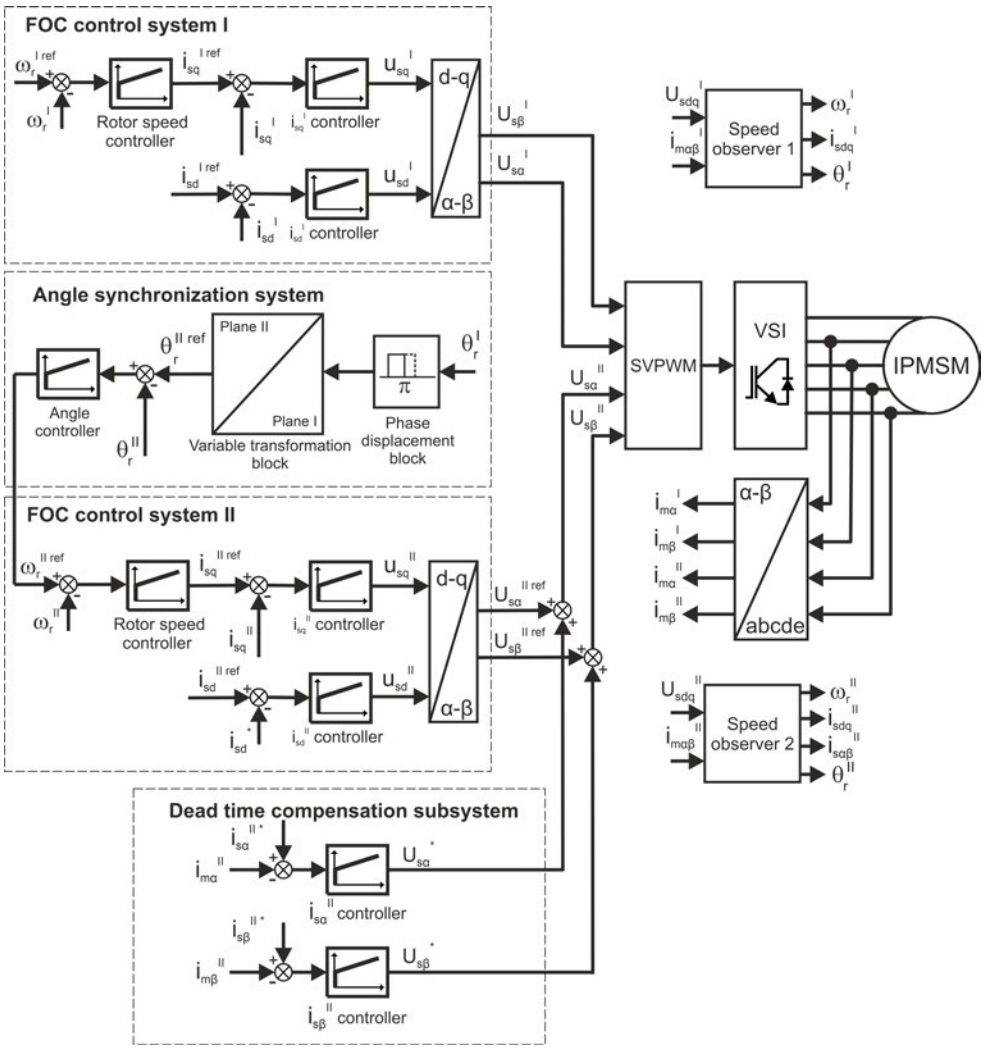

Fig. 1. The structure of the proposed control system with a 5-phase IPMSM and dead-time effect compensation

The nature of a five-phase machine with concentrated windings [1] allows one to operate in two modes, with and without the third harmonic injection. The proposed FOC control system can fully utilize this feature, so two control scenarios were prepared for these modes:

1. Sinusoidal, without the third harmonic injection (voltage generated only in the I plane, while in the II plane: $U_{s\alpha}^{\mathrm{ref}} = 0$, $U_{s\beta}^{\mathrm{ref}} = 0$),
2. Trapezoidal, with the injection of the third harmonic (voltage generated in both I and II planes).

The purpose of the proposed method is to minimize the dead-time effects in both operating modes by injecting additional reference voltage components in the II plane.

2.2. Proposed dead-time effect compensation method

In order to compensate the dead-time effects, an additional subsystem was added to the control scheme (Fig. 1). It consists of two current controllers in $\alpha - \beta$ coordinates. The control system used utilizes phase current measurements at the output of the inverter and their subsequent Clarke transformation into two sets of $\alpha - \beta$ components, each mapped to a separate coordinate system: $i^{\mathrm{I}}_{m\alpha}$, $i^{\mathrm{I}}_{m\beta}$ for the I, and $i^{\mathrm{II}}_{m\alpha}$, $i^{\mathrm{II}}_{m\beta}$, for the II plane. The measured third harmonic current components are used as feedback for the dead-time compensation subsystem, as it was noticed that the unwanted disturbances due to the dead-time effects appear only in the II plane. The controllers generate $\alpha - \beta$ reference voltage components: $U^{\mathrm{II}^*}_{s\alpha}$, $U^{\mathrm{II}^*}_{s\beta}$, which are added to the reference voltage components generated by the FOC control system in plane II in order to minimize the unwanted disturbances caused by the dead-time influence.

In the first mode of operation, with sinusoidal voltage supply, as the purpose of the proposed method is to generate sinusoidal phase currents with no low-order harmonic content, the FOC control system in plane II does not generate any reference voltage components. Simultaneously, the dead-time effect compensation block introduces the additional third harmonic voltage injection. For this purpose the reference current components for the third harmonic are set for: $i^{\mathrm{I}^*}_{s\alpha} = 0$, $i^{\mathrm{I}^*}_{s\beta} = 0$, so that the controllers generate reference voltages $U^{\mathrm{I}^*}_{s\alpha}$, $U^{\mathrm{II}^*}_{s\beta}$, minimizing the current in the II plane.

When operating in the second mode, with trapezoidal voltage supply, the FOC control system in the II plane generates the reference voltage components for the purpose of third harmonic injection. Just as in the case of sinusoidal supply, the dead-time effect compensation block introduces the additional third harmonic injection. This time the reference current values are set for: $i^{\mathrm{II}^*}_{s\alpha} = i^{\mathrm{II}}_{s\alpha}$, $i^{\mathrm{II}^*}_{s\beta} = i^{\mathrm{II}}_{s\beta}$, where $i^{\mathrm{II}}_{s\alpha}$ and $i^{\mathrm{II}}_{s\beta}$ are the currents estimated by the state observer. In this case the unwanted harmonics have been reduced, so only the required third harmonic content will be present.

The reference and measured values of the $\alpha - \beta$ current components in the II plane are used to calculate the current error values:

$$\mathrm{error}\_i^{\mathrm{II}}_{s\alpha} = i^{\mathrm{II}^*}_{s\alpha} - i^{\mathrm{II}}_{m\alpha}, \tag{1}$$

$$\mathrm{error}\_i^{\mathrm{II}}_{s\beta} = i^{\mathrm{II}^*}_{s\beta} - i^{\mathrm{II}}_{m\beta}. \tag{2}$$

Utilizing (1) and (2) the PI controllers calculate voltage components: $U^{\mathrm{II}^*}_{s\alpha}$, $U^{\mathrm{II}^*}_{s\beta}$. Both controllers have the same gains of: $K_p = 2.5$, $K_i = 0.05$.

The operation of the dead-time compensation subsystem in two modes of operation can be defined by the following condition:

$$\begin{aligned} i^{\mathrm{II}^*}_{s\alpha} &= \begin{cases} 0 & \text{if } \left(U^{\mathrm{II}^{\mathrm{ref}}}_{s\alpha} = 0\right) \\ i^{\mathrm{II}}_{s\alpha} & \text{if } \left(U^{\mathrm{II}^{\mathrm{ref}}}_{s\alpha} \neq 0\right) \end{cases}, \\ i^{\mathrm{II}^*}_{s\beta} &= \begin{cases} 0 & \text{if } \left(U^{\mathrm{II}^{\mathrm{ref}}}_{s\beta} = 0\right) \\ i^{\mathrm{II}}_{s\beta} & \text{if } \left(U^{\mathrm{II}^{\mathrm{ref}}}_{s\beta} \neq 0\right) \end{cases}. \end{aligned} \tag{3}$$

3. Experimental setup

The proposed control system was tested on a test setup assembled in the laboratory. The laboratory setup consists of the prototype five-phase IPMSM, supplied by a five-phase inverter, connected by a common shaft with a three-phase squirrel-cage induction machine generating the load torque. The inverters powering both motors are connected to a PC via a USB cable and controlled using a dedicated software package. The view of the drive unit is shown in Fig. 2.

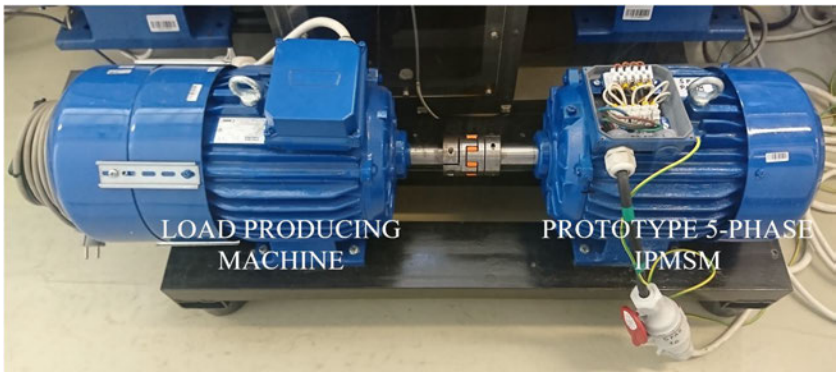

Fig. 2. Drive system with a five-phase IPMSM (on the right)

The parameters of the prototype five-phase IPMSM are listed in Table 1, while the parameters of the prototype inverter are listed in Table 2:

Table 1. Parameters of the prototype five-phase IPMSM

Parameter name	**Symbol**	**Value**	**Unit**
Rated power	P_n	5 500	W
Nominal phase voltage	U_n	140	V
Nominal phase current	I_n	10.2	A
Number of pole pairs	p	3	–
Nominal frequency	f_n	75	Hz
Stator resistance	R_s	0.816	Ω
Stator d-axis inductance	L_d	10.85	mH
Stator q-axis inductance	L_q	16.5	mH

The view of the prototype five-phase inverter is shown in Fig. 3.

The dead time without the compensation method was set for 2 µs.

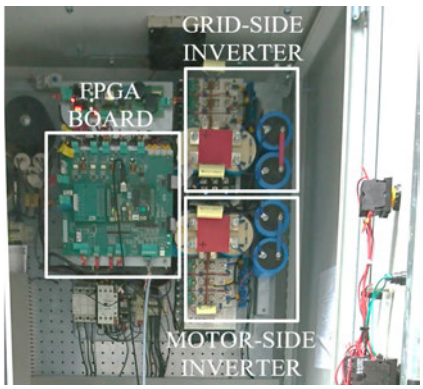

Fig. 3. View of the prototype five-phase inverter

Table 2. Parameters of the prototype five-phase inverter

Parameter name	Symbol	Value	Unit
DC-link voltage	U_{DC}	538	V
Capacitors in DC-link	C	2×100	μF
IGBT transistor	type	MMG50SR120B	–
FPGA Altera Cyclone II	type	EP2C8F256	–
DSP Control Board	type	ADSP21363	–
Switching frequency	f_s	3.33	kHz

4. Experimental studies

In order to verify the correct performance of the proposed dead-time compensation method a number of experimental tests were carried out.

4.1. Experimental tests with sinusoidal supply

The first part of the experimental research was carried out in the first mode of operation of the control system, i.e. with sinusoidal supply. The tests consisted of recording and analyzing the values of: phase current (i_{mA}), measured current α components in the I ($i^{\mathrm{I}}_{m\alpha}$) and II plane ($i^{\mathrm{II}}_{m\alpha}$) and the reference voltage α components in the I ($u^{\mathrm{I}}_{s\alpha}$) and II plane ($u^{\mathrm{II}}_{s\alpha}$). The waveforms were recorded in a steady state for three different values of the reference rotor speed. Figures 4–6 present the recorded waveforms for different speed values of $\omega^{\mathrm{ref}} = 0.3$, 0.5 and 0.8 [p.u.] for Figs. 4, 5 and 6, respectively.

The amplitude of the third harmonic current component is significantly reduced by the proposed compensation scheme (by up to 2.5 times for $\omega^{\mathrm{ref}} = 0.8$). The output phase current waveforms after the compensation are much closer to purely sinusoidal waveforms.

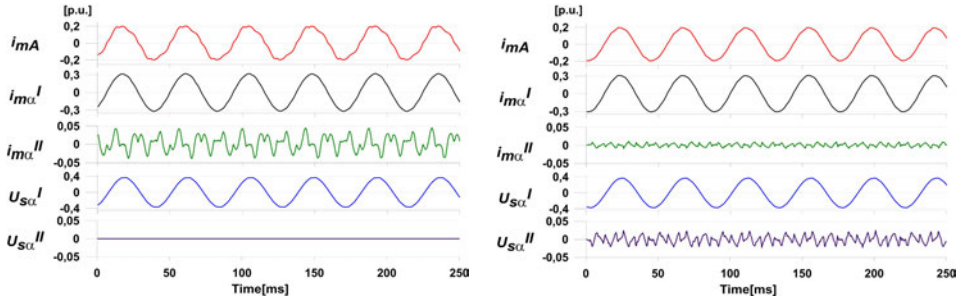

(a) (b)

Fig. 4. Phase voltage and current components for a reference speed of $\omega^{\text{ref}} = 0.3$ p.u.: (a) without compensation; (b) with compensation

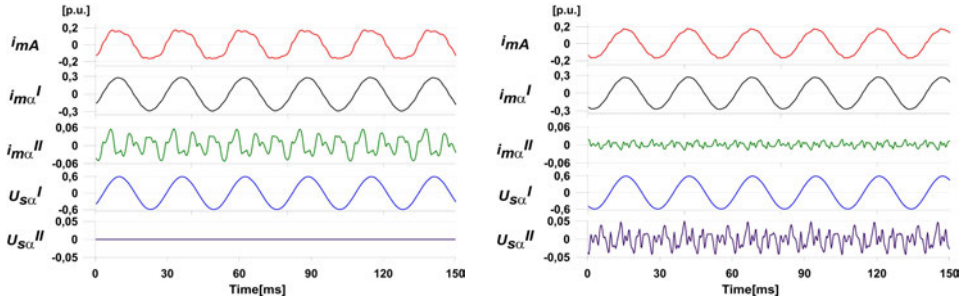

(a) (b)

Fig. 5. Phase voltage and current components for a reference speed of $\omega^{\text{ref}} = 0.5$ p.u.: (a) without compensation; (b) with compensation

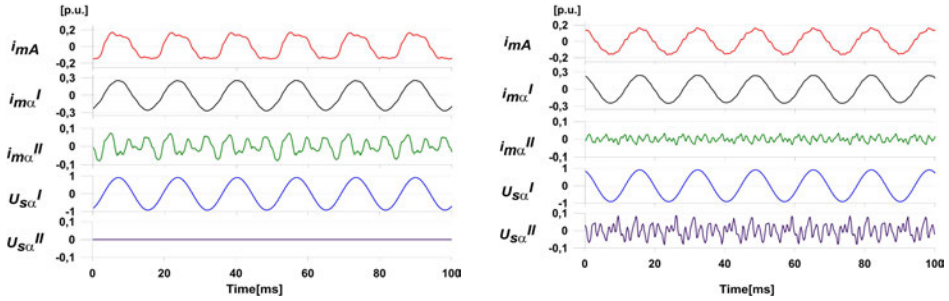

(a) (b)

Fig. 6. Phase voltage and current components for a reference speed of $\omega^{\text{ref}} = 0.8$ p.u.: (a) without compensation; (b) with compensation

The next part of the research consisted of frequency analysis of phase current and line-to-line voltage in a steady state for three different values of reference rotor speed. Fast Fourier transform (FFT) and total harmonic distortion (THD) analyses were performed for each reference speed, both with and without dead-time compensation. Figures 7–9 present the recorded phase current waveforms and their FFT spectra.

Figures 10–12 present the phase current THD values obtained during the conducted experimental tests. The THD value was calculated using a Tektronics oscilloscope, while the maximum number of analyzed harmonics was set to 100.

The obtained phase current waveforms confirm the benefits of the proposed dead-time effect compensation method. Comparing the current waveforms with and without dead-time effect compensation, (Figs. 4–6), the proposed method allows one to achieve phase currents significantly closer to purely sinusoidal. This visual impression is confirmed by the phase current FFT spectra as the magnitudes of the unwanted low-order harmonics are substantially reduced.

Figure 13(a) presents a bar diagram of the phase current THD-F values for each reference speed. The proposed dead-time effect compensation method allows for achieving up to 3 times lower harmonic distortion (for the reference speed of $\omega^{\text{ref}} = 0.8$ p.u.).

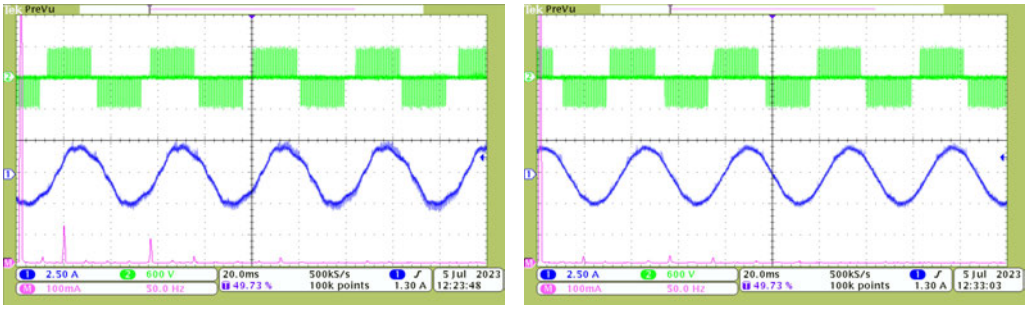

(a) (b)

Fig. 7. Phase current waveform and FFT for a reference speed of $\omega^{\text{ref}} = 0.3$ p.u.: (a) without compensation: (b) with compensation

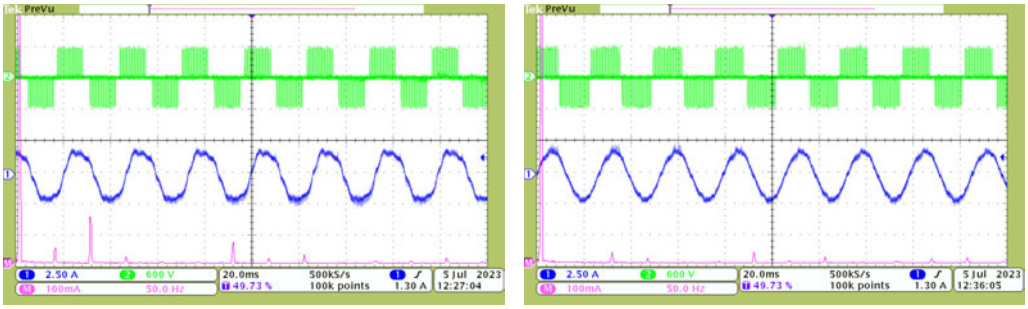

(a) (b)

Fig. 8. Phase current waveform and FFT for a reference speed of $\omega^{\text{ref}} = 0.5$ p.u.: (a) without compensation; (b) with compensation

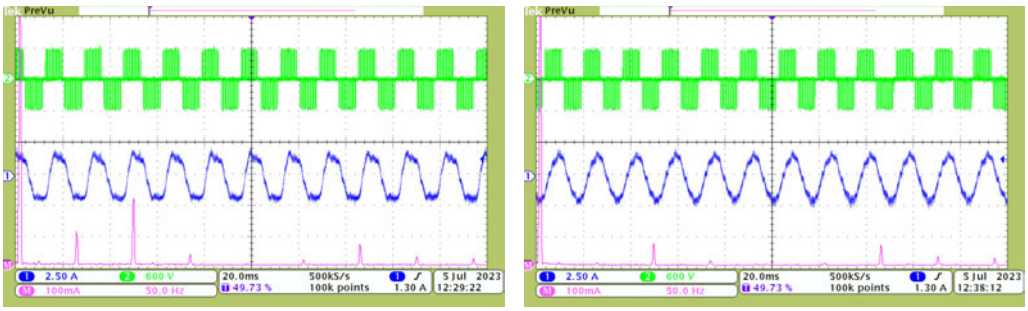

(a) (b)

Fig. 9. Phase current waveform and FFT for a reference speed of $\omega^{\text{ref}} = 0.8$ p.u.: (a) without compensation; (b) with compensation

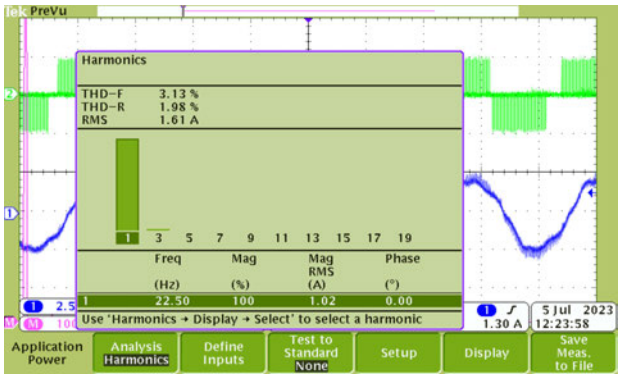

(a)

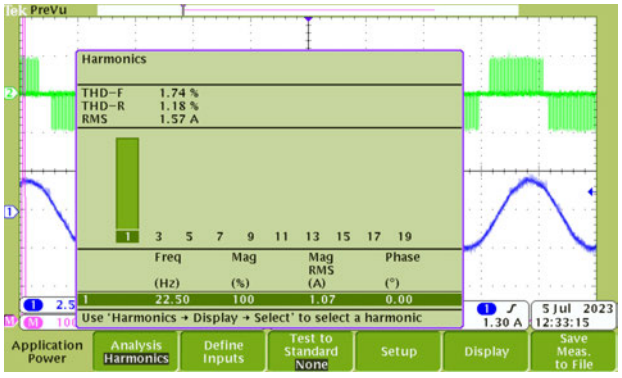

(b)

Fig. 10. Phase current THD for a reference speed of $\omega^{\text{ref}} = 0.3$ p.u.: (a) without compensation; (b) with compensation

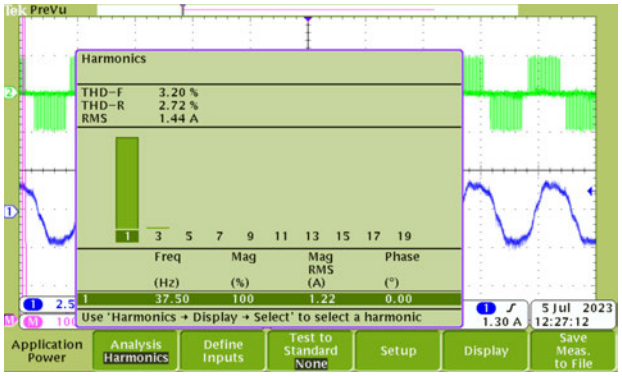

(a)

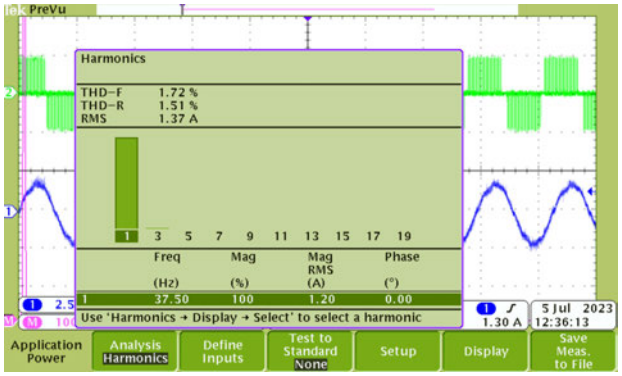

(b)

Fig. 11. Phase current THD for a reference speed of $\omega^{\text{ref}} = 0.5$ p.u.: (a) without compensation; (b) with compensation

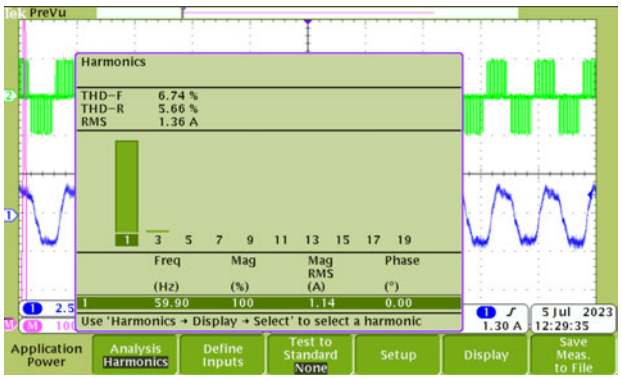

(a)

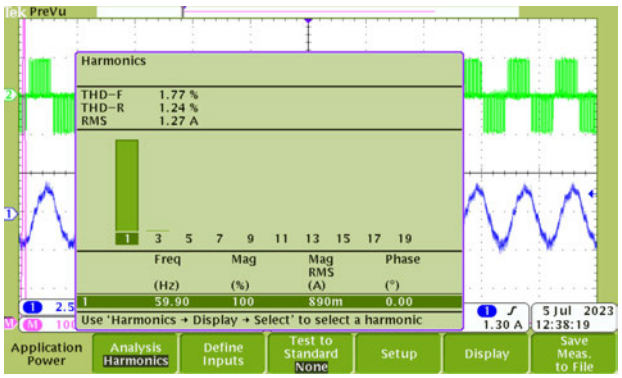

(b)

Fig. 12. Phase current THD for a reference speed of $\omega^{\text{ref}} = 0.8$ p.u.: (a) without compensation; (b) with compensation

Figure 13(b) presents a bar diagram of the line-to-line THD-F values for each reference speed.

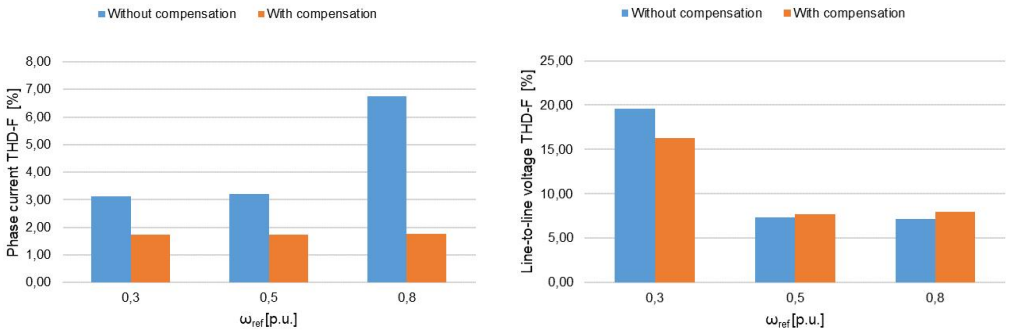

(a) (b)

Fig. 13. THD-F values of: (a) phase current; (b) line-to-line voltage, for different reference speed values with and without compensation (sinusoidal supply)

The obtained values are relatively similar with and without compensation. The proposed control scheme has shown better result for lower and slightly worse for the higher speed values. The increase in the voltage THD-F can be explained by the necessity of the third harmonic voltage components' injection.

4.2. Experimental tests with trapezoidal supply

The second part of the experimental research was carried out in the second mode of operation, with trapezoidal voltage supply. The FFT and THD analyses of the waveforms of phase current in a steady state, for three different values of reference rotor speed, were performed. Figures 14–16 present the recorded phase current waveforms and their FFT spectra with and without the dead-time effect compensation.

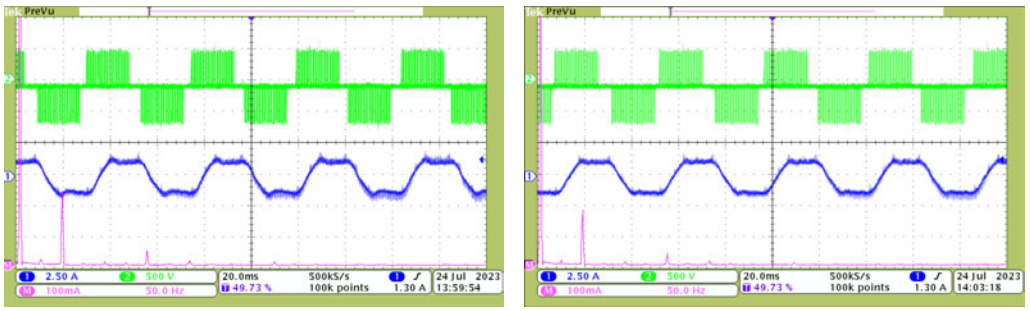

(a) (b)

Fig. 14. Phase current waveform and FFT for a reference speed of $\omega^{\text{ref}} = 0.3$ p.u.: (a) without compensation; (b) with compensation

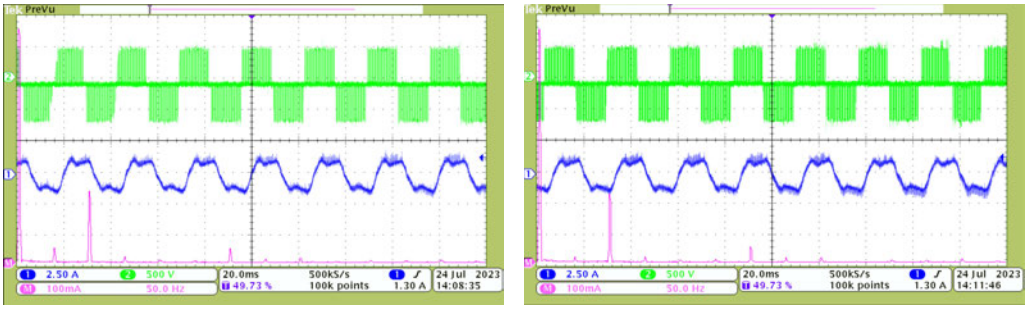

(a) (b)

Fig. 15. Phase current waveform and FFT for a reference speed of $\omega^{\text{ref}} = 0.5$ p.u.: (a) without compensation; (b) with compensation

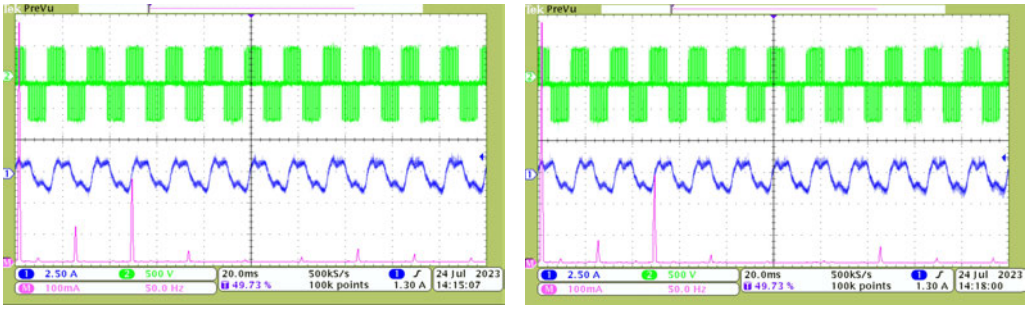

(a) (b)

Fig. 16. Phase current waveform and FFT for a reference speed of $\omega^{\text{ref}} = 0.8$ p.u.: (a) without compensation; (b) with compensation

Figures 17–19 present the phase current THD values obtained during the second part of the experimental tests.

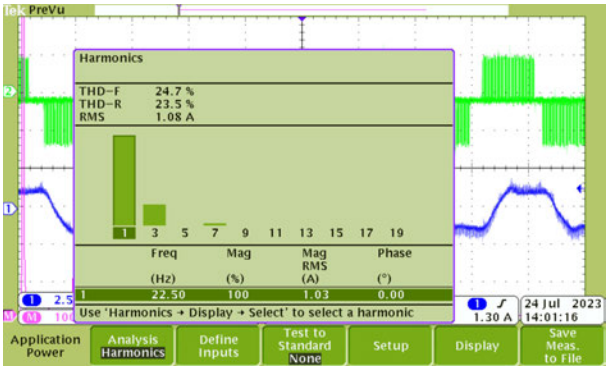

(a)

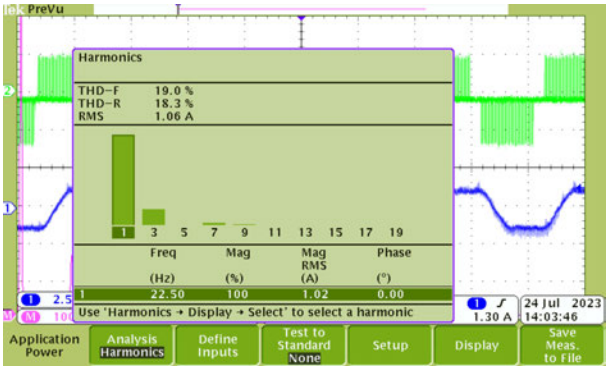

(b)

Fig. 17. Phase current THD for a reference speed of $\omega^{\text{ref}} = 0.3$ p.u.: (a) without compensation; (b) with compensation

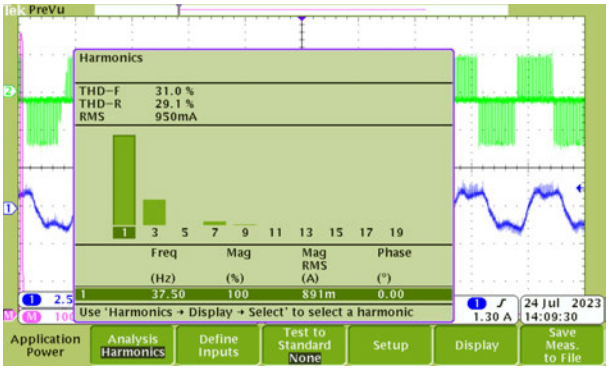

(a)

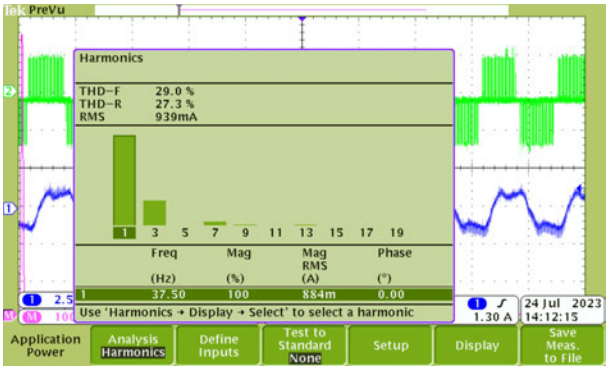

(b)

Fig. 18. Phase current THD for a reference speed of $\omega^{\text{ref}} = 0.5$ p.u.: (a) without compensation; (b) with compensation

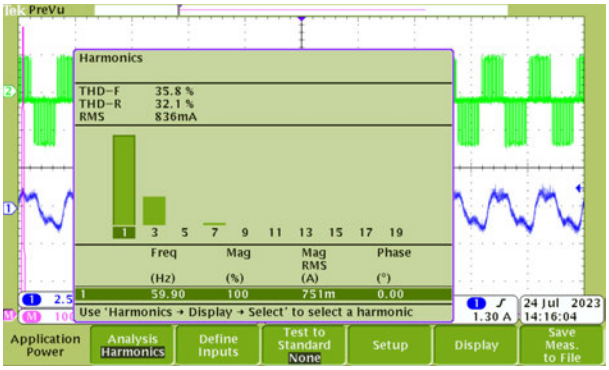

(a)

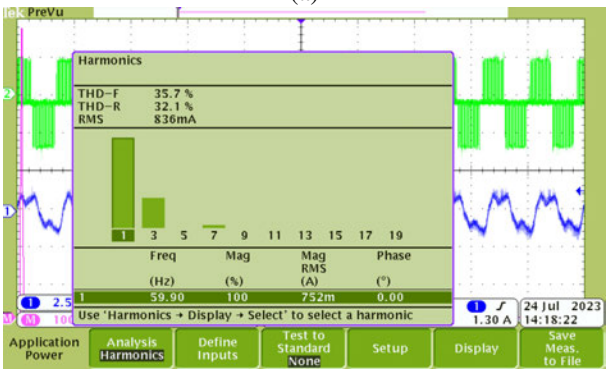

(b)

Fig. 19. Phase current THD for a reference speed of $\omega^{\text{ref}} = 0.8$ p.u.: (a) without compensation; (b) with compensation

The obtained phase current waveforms confirm the improvements achieved thanks to the proposed dead-time effect compensation method. Comparing the current waveforms and their FFT spectra and THD values with and without dead-time effect compensation, (Figs. 14–19), the proposed method shows noticeable improvement under low reference speed operation (THD value was reduced from 24.7% to 19.0%). For higher speed values the results are quite similar due to the nature of dead-time effects, as the dead-time influence is the highest for a low frequency.

Figure 20 presents the bar graph analysis of the THD-F spectra for phase current (Fig. 20(a)) and line-to-line voltage (Fig. 20(b)) for trapezoidal supply mode. The phase current THD-F values have been reduced for smaller reference speed values, but remained at a similar level for the reference speed of $\omega^{\text{ref}} = 0.8$ p.u.

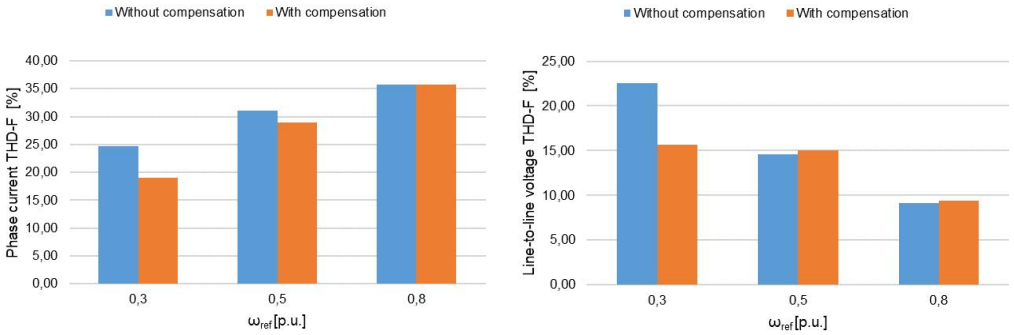

Fig. 20. THD-F values of: (a) phase current; (b) line-to-line voltage, for different reference speed values with and without compensation (trapezoidal supply)

In the case of line-to-line voltage the results are comparable to those achieved for sinusoidal supply (better result for lower and slightly worse for the higher speed values).

It is worth noticing that much higher THD values obtained for the trapezoidal supply can be explained by the fact that as the THD analyses treat all the harmonic content higher than the basic harmonic as distortion, the 3$^{\text{rd}}$ harmonic content injected for the purpose of torque enhancement is also treated as a disturbance as well, so in the case of trapezoidal supply the amount of THD due to the dead-time effects is much lower.

The last part of the experimental research consisted of estimating the increase in computational burden caused by the addition of the dead-time compensation subsystem. An additional function was added to the code to calculate the control program execution time. It was established that it has increased from 10.26 ms for no compensation to 10.45 ms with the compensation subsystem added.

5. Conclusions

The results of the experimental research performed prove the effectiveness of the proposed dead-time effect compensation scheme. The waveforms of the phase currents after the compensation, recorded during the first part of the experimental tests, are significantly closer to purely sinusoidal

than in the default control scheme in the whole speed range. The amplitude of the third harmonic current components is reduced by up to 2.5 times when compared to the system without the compensation subsystem. The results of the FFT and THD analyses performed for the phase current waveforms confirm the correct operation of the compensation system, as the magnitudes of the unwanted low-order harmonics are significantly reduced. The decrease in the THD is especially visible for the higher speed values (up to 3 times lower harmonic distortion for the reference speed of 0.8 p.u.).The difference in the voltage THD is not significant compared to the achieved improvement in the current THD.

In the case of trapezoidal voltage, supply the main difference between conventional and the proposed schemes is visible for low-speed operation. The obtained results prove that the proposed solution allows for achieving a lower current THD (by up to 23% for a reference speed of 0.3 p.u.) while the possibility of independent output voltage generation in the I and II planes is retained.

The proposed method introduces additional current controllers operating in the $\alpha - \beta$ fixed orthogonal coordinate system, which does not further complicate the structure of the control system by adding an additional Park transformation, as the measured current components in α-β coordinates are already available. The increase of the control program execution time from 10.26 ms for no compensation to 10.45 ms with compensation amounts to an increase of 1.85%. Such an increase is negligible and does not negatively affect the system's performance, especially when compared to the benefits gained.

However, there is a limitation of the proposed dead-time effect compensation method resulting from the additional delay caused by the PI current controllers. These delays become noticeable at higher frequency values. The introduction of a different type of current controllers, e.g. hysteresis or predictive controllers, could further improve the proposed dead-time effect compensation strategy.

Acknowledgements

This research was funded in whole by National Science Centre, Poland under Grant 2021/41/N/ST7/01968. For the purpose of Open Access, the author has applied a CC-BY public copyright licence to any Author Accepted Manuscript (AAM) version arising from this submission.

References

[1] Levi E., Bojoi R., Profumo F., Toliyat H.A., Williamson S., *Multiphase induction motor drives – a technology status review*, Electric Power Applications IET, vol. 1, no. 4, pp. 489–516 (2007), DOI: 10.1049/iet-epa:20060342.

[2] Levi E., *Multiphase Electric Machines for Variable-Speed Applications*, IEEE Transactions on Industrial Electronics, vol. 55, no. 5, pp. 1893–1909 (2008), DOI: 10.1109/TIE.2008.918488.

[3] Cao W., Mecrow B.C., Atkinson G.J., Bennett J.W., Atkinson D.J., *Overview of Electric Motor Technologies Used for More Electric Aircraft (MEA)*, IEEE Transactions on Industrial Electronics, vol. 59, no. 9, pp. 3523–3531 (2012), DOI: 10.1109/TIE.2011.2165453.

[4] Barrero F., Duran M.J., *Recent Advances in the Design, Modeling, and Control of Multiphase Machines – Part I*, IEEE Transactions on Industrial Electronics, vol. 63, no. 1, pp. 449–458 (2016), DOI: 10.1109/TIE.2015.2447733.

[5] Zhang J., He S.J., Wang K., *Multi-Harmonic Currents Control Strategy for Five-Phase Permanent Magnet Machine with non-sinusoidal back-EMF*, IEEE Access (2020), DOI: 10.1109/ACCESS.2020.2989323.

[6] Laksar J., Cermak R., Drazan J., *Comparison of Five-Phase Winding Configurations of High-Speed PMSM Feasible to the Third Harmonic Current Injection*, 2022 20th International Conference on Mechatronics – Mechatronika (ME), Pilsen, Czech Republic, pp. 1–7 (2022), DOI: 10.1109/ME54704.2022.9983381.

[7] Lewicki A., *Dead-Time Effect Compensation Based on Additional Phase Current Measurements*, IEEE Transactions on Industrial Electronics, vol. 62, no. 7, pp. 4078–4085 (2015), DOI: 10.1109/TIE.2015.2389756.

[8] Szwarc K.J., Cichowski A., Nieznanski J., Szczepankowski P., *Modeling the effect of parasitic capacitances on the dead-time distortion in multilevel NPC inverters*, IEEE International Symposium on Industrial Electronics, Gdansk, Poland, pp. 1869–1874 (2011), DOI: 10.1109/ISIE.2011.5984442.

[9] Attia H., Che H.S., Suan F.T., Elkhateb A., *Mitigating the Dead-time Effects on Harmonics Spectrum of Inverter Waveform by the Confined Band VSFPWM Technique*, International Journal of Power Electronics and Drive Systems (IJPEDS), vol. 12, no. 1, pp. 295–303 (2021), DOI: 10.11591/ijpeds.v12.i1.pp295-303.

[10] Cheng J., Chen D., Chen G., *Modeling and Compensation for Dead-Time Effect in High Power IGBT/IGCT Converters with SHE-PWM Modulation*, Energies, vol. 13, no. 17, 4348 (2020), DOI: 10.3390/en13174348.

[11] Li C. *et al*., *Analysis and compensation of dead-time effect considering parasitic capacitance and ripple current*, 2015 IEEE Applied Power Electronics Conference and Exposition (APEC), Charlotte, NC, USA, pp. 1501–1506 (2015), DOI: 10.1109/APEC.2015.7104546.

[12] Wan W., Yu T., Duan S., *Dead-Time Compensation in Active NPC Three-Level Inverters Considering Current Ripple*, IEEE Transactions on Transportation Electrification, vol. 9, no. 1, pp. 1189–1199 (2023), DOI: 10.1109/TTE.2022.3164891.

[13] Han D., Peng F.Z., Dwari S., *Eliminating Dead-Time Effects with Zero-Current Clamping Control for WBG Multilevel Inverters*, 2021 IEEE Applied Power Electronics Conference and Exposition (APEC), Phoenix, AZ, USA, pp. 542–548 (2021), DOI: 10.1109/APEC42165.2021.9487434.

[14] Piao C., Hung J.Y., *Analysis and compensation of Dead-time effect in multi-level diode clamped VSI based on simplified SVPWM*, 2015 IEEE 10th Conference on Industrial Electronics and Applications (ICIEA), Auckland, New Zealand, pp. 375–380 (2015), DOI: 10.1109/ICIEA.2015.7334142.

[15] Miao Z., Wei J., Guo T., Zheng M., *Dead-time Compensation Method Based on Field Oriented Control Strategy*, IOP Conference Series: Earth and Environmental Science, vol. 358, no. 4, 042049 (2019), DOI: 10.1088/1755-1315/358/4/042049.

[16] Jin S., Zhang W., Liu Z., Xie F., Xu Y., Zou J., *Direct-axis Dead-time Effect Compensation Strategy Based on Adaptive Linear Neuron Method for PMSM Drives*, IECON 2022 – 48th Annual Conference of the IEEE Industrial Electronics Society, Brussels, Belgium, pp. 1–6 (2022), DOI: 10.1109/IECON49645.2022.9968832.

[17] Yi-Chieh Pai, Jun-Ping Chang, Ming-Yang Cheng, Tsorng-Juu Liang, *Dead-time effects compensation for PMSM drives – an adaptive linear neuron approach*, 2017 IEEE 3rd International Future Energy Electronics Conference and ECCE Asia (IFEEC 2017 – ECCE Asia), Kaohsiung, Taiwan, pp. 1025–1030 (2017), DOI: 10.1109/IFEEC.2017.7992182.

[18] Lang J., Tong C., Zheng P., Liang X., Yuan X., Ren W., *Dead-Time Effect Analysis and Compensation for Deadbeat-Direct Torque and Flux Control of PMSMs to Eliminate Steady-State Error*, 2022 25th International Conference on Electrical Machines and Systems (ICEMS), Chiang Mai, Thailand, pp. 1–5 (2022), DOI: 10.1109/ICEMS56177.2022.9983020.

[19] Jones M., Dujic D., Levi E., Vukosavic S.N., *Dead-time effects in voltage source inverter fed multi-phase AC motor drives and their compensation*, 2009 13th European Conference on Power Electronics and Applications, Barcelona, Spain, pp. P.1–P.10 (2009).

[20] Iqbal A., Levi E., *Space vector modulation schemes for a five-phase voltage source inverter*, 2005 European Conference on Power Electronics and Applications, Dresden, Germany, 9035837 (2005), DOI: 10.1109/EPE.2005.219194.

[21] Dujic D., Levi E., Jones M., Grandi G., Serra G., Tani A., *Continuous PWM Techniques for Sinusoidal Voltage Generation with Seven-Phase Voltage Source Inverters*, 2007 IEEE Power Electronics Specialists Conference, Orlando, FL, USA, pp. 47–52 (2007), DOI: 10.1109/PESC.2007.4341959.

[22] Guzinski J. *et al*., *Sensorless multiscalar control of five-phase induction machine with inverter output filter*, 2017 19th European Conference on Power Electronics and Applications (EPE'17 ECCE Europe), Warsaw, Poland, pp. P.1–P.10 (2017), DOI: 10.23919/EPE17ECCEEurope.2017.8099186.

[23] Adamowicz M., Guzinski J., Krzeminski Z., *Nonlinear control of five phase induction motor with synchronized third harmonic flux injection*, 2015 First Workshop on Smart Grid and Renewable Energy (SGRE), Doha, Qatar, pp. 1–6 (2015), DOI: 10.1109/SGRE.2015.7208727.

[24] Morawiec M., Kroplewski P., Odeh C., *Nonadaptive Rotor Speed Estimation of Induction Machine in an Adaptive Full-Order Observer*, IEEE Transactions on Industrial Electronics, vol. 69, no. 3, pp. 2333–2344 (2022), DOI: 10.1109/TIE.2021.3066919.

[25] Volpato Filho C.J., Vieira R.P., *Adaptive Full-Order Observer Analysis and Design for Sensorless Interior Permanent Magnet Synchronous Motors Drives*, IEEE Transactions on Industrial Electronics, vol. 68, no. 8, pp. 6527–6536 (2021), DOI: 10.1109/TIE.2020.3007101.